Dynamics of matter-wave solitons in a time-modulated two-dimensional optical lattice.

Gennadiy Burlak
Centro de Investigación en Ingeniería y Ciencias Aplicadas, Universidad Autónoma del Estado de Morelos, Cuernavaca, Mor. México

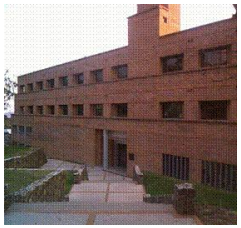

First let me remind some *simple* properties of Bose particles. The number of Bose noninteracting particles is:

$$N = \sum_k \left[\exp(\frac{\varepsilon_k - \mu}{T}) - 1 \right]^{-1}, \tag{1}$$

where $\varepsilon_k = \hbar^2 k^2 / 2m$ is energy, and μ is chemical potential. To calculate the transition temperature T_0, we replace in Eq.(1) the sum with the integral over all momentum states $p = \hbar k$, $k = [2m\varepsilon]^{1/2} / \hbar$, $z = \varepsilon / T$, that allows to rewrite N as

$$\frac{N}{V} = C \int_0^\infty z^{1/2} dz / \left[\exp(z - \frac{\mu}{T}) - 1 \right] \tag{2}$$

where $C = C(T)$, V is volume. From Eq.(2) μ can be interpreted as the implicit function of T and N/V as $\mu = \mu(T, N/V) \leq 0$. For $\mu = 0$ the integral Eq.(2) defines the critical temperature $T = T_0$ and the particle number corresponding to the negligible chemical potential conditions $\mu = 0$.

Simple Einstein's argument (see e.g. L.Landau, E.Lifshitc, Statistical physics, V.5) shows that for $T \leq T_0$ the number of *noninteracting* particles N can be rewritten as $N = N_{\varepsilon>0} + N_{\varepsilon=0}$, where $N_{\varepsilon>0} = (T/T_0)^{3/2} N$ is the particle number with $\varepsilon > 0$, while $N_{\varepsilon=0} = \left[1 - (T/T_0)^{3/2}\right] N$ is the number of particles in the ground state energy $\varepsilon = 0$. Thus, if $T \to 0$ than $N_{\varepsilon=0} \to N$, so all the Bose particles transit to the ground state with $\varepsilon = 0$ (Bose-Einstein condensate - BEC).

This is a simple conclusion of the ideal *noninteracting* particles model. This state of matter was first predicted by Satyendra Nath Bose and Albert Einstein in 1924 -25.

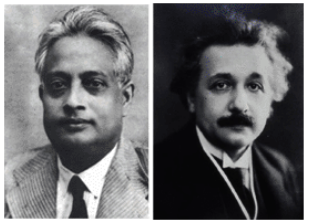

What happens in a real situation with the *interacting* particles?

A Bose–Einstein condensate (BEC) is a state of matter of a dilute gas of weakly interacting bosons confined in an external potential and cooled to temperatures very near absolute zero (0 K or -273.15 °C). Under such conditions, a large fraction of the bosons occupy the *lowest quantum state* of the external potential, at which point quantum effects become apparent on *a macroscopic scale*.

The first gaseous condensate was produced by Eric Cornell and Carl Wieman in 1995 at the University of Colorado at Boulder NIST-JILA lab, using a gas of rubidium atoms cooled to 170 nanokelvin (nK) (1.7×10^{-7} K). For their achievements Cornell, Wieman, and Wolfgang Ketterle at MIT received the 2001 *Nobel Prize in Physics*.

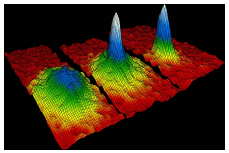

The state of the BEC can be described by the wavefunction of the condensate $\psi(r)$, so $|\psi(r)|^2$ is interpreted as the particle density, so the *total number of atoms* is $N = \int dr\, |\psi(r)|^2 = \|\psi\|^2$. Provided essentially all atoms are in the condensate (that is, have condensed to the ground state), and treating the bosons using mean field theory, the energy E associated with the state $\psi(r)$ is:

$$E = \int dr \left[\frac{\hbar^2}{2m} |\nabla \psi(r)|^2 + V(r) |\psi(r)|^2 + \frac{1}{2} G |\psi(r)|^4 \right] \tag{3}$$

Minimising this energy with respect to variations $\delta\psi(r)$, and holding the number of atoms constant, yields the *Gross-Pitaevskii* equation (GPE) (also a *non-linear Schrödinger equation)*:

$$i\hbar \frac{\partial \psi(r)}{\partial t} = \left(-\frac{\hbar^2 \nabla^2}{2m} + V(r) + G |\psi(r)|^2 \right) \psi(r) \tag{4}$$

that normally applied for theoretical analysis.

A challenging subject in the study of dynamical patterns in Bose-Einstein condensates (BECs) is the investigation of *matter-wave solitons* in multidimensional settings. Various routes leading to the creation of stable 2D and 3D solitons have been elaborated theoretically. The proposed approaches have much in common with their counterparts developed for the stabilization of 2D and 3D spatiotemporal solitons in *nonlinear optics*, see review [2].

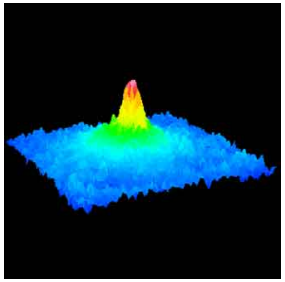

Nonlinear Schrödinger equation (NSE)

$$i\frac{\partial \Phi}{\partial \tau} = [-\nabla_{\perp}^2 + V(\mathbf{r}) + G\,|\Phi|^2]\Phi, \tag{5}$$

where G is a real function (the nonlinear coefficient), so that if $G > 0$ the nonlinearity is *repulsive*, whereas for $G < 0$ the nonlinearity is *attractive*.

It is well known that for $G < 0$, and if $N = \|u0\|^2$ is above a threshold value N_c, the solutions of this equation can self-focus and become *singular* in a finite time. This phenomenon is called *wave collapse or blowup of the wave amplitude*.
When $G < 0$, there exists only one solution of NSE which is real, positive and radially symmetric and for which $\|u0\|^2$ has the minimum value and this solution *decays exponentially at infinity*. This solution is called the ground state or *Townes soliton*.

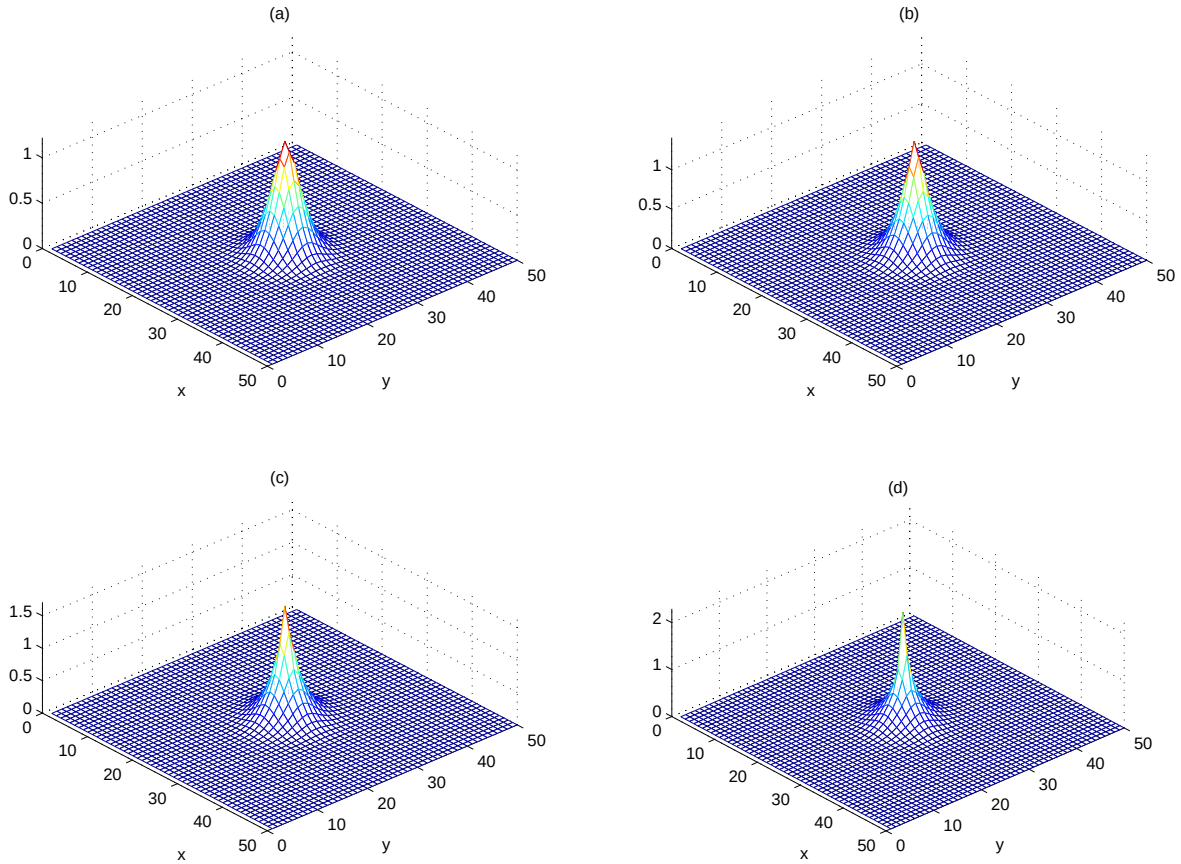

Figure: 1. Self-compressing of initial Gaussian package at *attractive* interaction $G = -1$ and the period of π-phase shift $T_t = 8$. (a) $\tau = 15$; (b) 20; (c) 25; (d) 30.

From the theory of nonlinear Schrödinger equations it is known that the *Townes soliton* has exactly the critical power for blowup $N_c = \|u0\|^2 \simeq 5.85$ (for $G = -1$), therefore, it separates in some sense the region of *collapsing* and expanding solutions. Moreover, the *Townes soliton is unstable*, i.e. small perturbations of this solution lead to *either expansion of the initial data or blowup in finite time*.

In *nonlinear optics a spatial modulation* of the nonlinear coefficient of the optical material is used to *prevent such a collapse* so that the optical beam becomes collapsing and expanding in alternating regions and is *stabilized in average*. The same idea now has been used in the field of matter waves to obtain a *stable BEC soliton*.

Typical optical lattices

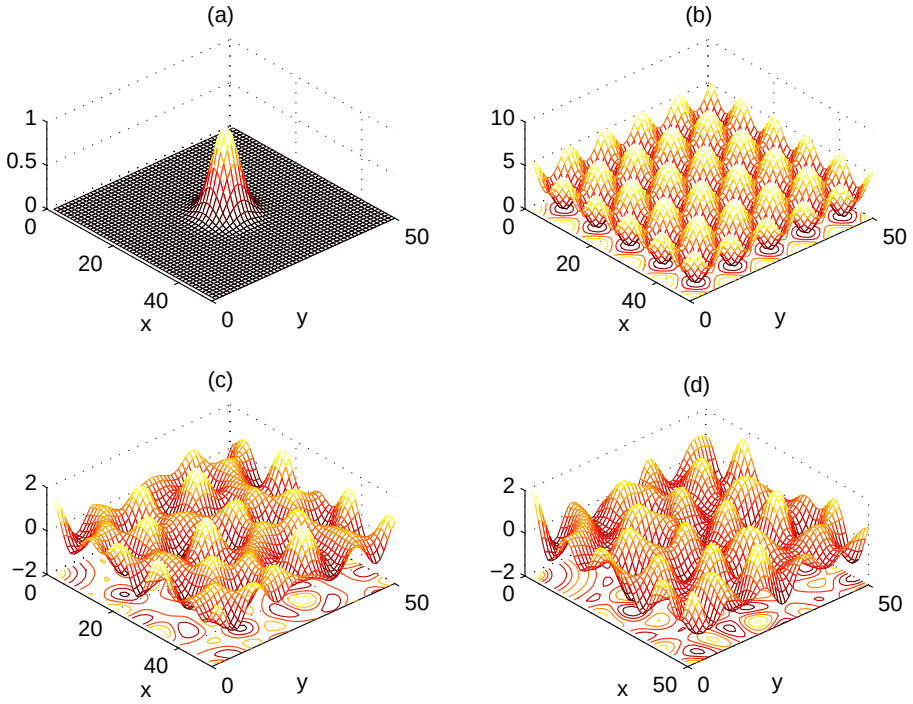

Figure: 2. (a) Init Gaussian package. (b),(c),(d) two-dimensional distribution of the trapping potential $V(x, y, 0)$ induced by optical lattices (OL) for Penrose tiling (a pattern of tiles, which completely cover an infinite plane in an *aperiodic* manner) for cases (b) $N = 4$; (c) $N = 5$; (d) $N = 7$.

2D Gross-Pitaevskii equation (GPE)

Thus, it is very important to construct soliton families and identify their stability boundaries in the 2D attractive model with the full 2D lattice subject to the time-periodic modulation. In the normalized form, the respective two-dimensional GPE for mean-field wave function $\Psi(x, y, t)$ is

$$i\frac{\partial \Psi}{\partial t} = -\frac{1}{2}\Delta_2\Psi - |\Psi|^2\Psi - V_0\left[1 + \frac{\varepsilon}{2}\cos(\omega t)\right]\left[\cos(2x) + \cos(2y)\right]\Psi, \tag{6}$$

where t is time, (x, y) are coordinates in the 2D plane (scaled so as to fix the OL period equal to π), and V_0 is the strength of the lattice, while ε and ω are the amplitude and frequency of its temporal modulation. Coefficient -1 in front of the nonlinear term in Eq. (6) implies that the nonlinearity is attractive [*G. Burlak, B. A. Malomed, "Dynamics of matter-wave solitons in a time-modulated two-dimensional optical lattice", Physical Review A. 77, 053606 (2008)*].

For a typical case of atoms of ^{7}Li loaded in the optical lattice (OL) with the period on the order of μm, a characteristic value of the scaled frequency, $\omega \sim 2$, corresponds, in physical units, to the modulation rate on the order of several KHz.

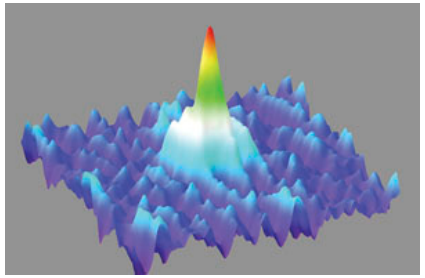

Lagrangian

Variational methods have been quite useful in many problems of nonlinear optics and BEC [38, 39, 4, 5, 18, 24]. To apply the VA to the present model, we notice that Eq. (6) can be derived from Lagrangian $L = \int_{-\infty}^{+\infty} \mathcal{L} dx$, with density

$$\mathcal{L} = \frac{i}{2}\left(\Psi^* \Psi_t - \Psi \Psi_t^*\right) - \frac{1}{2}\left(|\Psi_x|^2 + |\Psi_y|^2\right) + \frac{1}{2}|\Psi|^4 + V_0\left[1 + \frac{\varepsilon}{2}\cos(\omega t)\right]\left[\cos(2x) + \cos(2y)\right]|\Psi|^2, \quad (7)$$

where the asterisk stands for the complex conjugation. Following Refs. [4] and [5], we adopt the isotropic *ansatz* for the soliton,

$$\Psi_{\text{ans}}(x, y, t) = A(t) \exp\left(i\phi(t) + \frac{i}{2} b(t) r^2 - \frac{r^2}{2W^2(t)}\right), \quad (8)$$

where $r^2 \equiv x^2 + y^2$, and all variables $A(t)$, $\phi(t)$, $b(t)$, and $W(t)$ (amplitude, phase, radial *chirp*, and width, respectively) are real.

Effective Lagrangian

The substitution of the ansatz (8) in Eq. (7) and calculation of the integrals yield the effective Lagrangian,

$$L_{\rm eff} = -N\frac{d\phi}{dt} - \frac{N}{2W^2} + \frac{N^2}{4\pi W^2} + 2V_0\left[1+\frac{\varepsilon}{2}\cos(\omega t)\right]Ne^{-W^2} - \frac{1}{2}\frac{db}{dt}NW^2 - \frac{1}{2}b^2NW^2, \tag{9}$$

where $N \equiv \pi A^2 W^2$. The first Euler-Lagrange equation following from effective Lagrangian (9), $\delta\left(\int L_{\rm eff}dt\right)/\delta\phi = 0$ ($\delta/\delta\phi$ stands for the variational derivative of the action functional), is tantamount to the conservation of the norm of the wave function, which is the single dynamical invariant of Eq. (6). Indeed, the norm of ansatz (8) is

$$\int\int |\Psi_{\rm ans}(x,y)|^2\, dxdy = \pi A^2 W^2 \equiv N. \tag{10}$$

The second Euler-Lagrange equation

The second Euler-Lagrange equation, $\delta\left(\int L_{\rm eff}\,dt\right)/\delta b = 0$, reduces to the well-known expression for the chirp in terms of the time derivative of the width [38, 39], $b = W^{-1}\left(dW/dt\right)$. Using this relation, the next variational equation, which accounts to $\partial L_{\rm eff}/\partial\left(W^2\right) = 0$ [since Lagrangian (9) does not contain dW/dt] can be cast in the following final form,

$$\frac{d^2W}{dt^2} = \frac{1 - N/\tilde{N}_{\rm max}}{W^3} - 4V_0\left[1 + \frac{\varepsilon}{2}\cos(\omega t)\right] W \exp\left(-W^2\right), \quad (11)$$

where $\tilde{N}_{\rm max} \equiv 2\pi$ is the well-known VA prediction [38] for the critical (maximum) norm in the 2D space, which separates collapsing solutions at $N > \tilde{N}_{\rm max}$, i.e. with $W(t) \to 0,\ A(t) \to \infty$ at $t \to t_{\rm clps}$ [for $V_0 = 0$ and initial conditions $W(t=0) = W_0$ and $dW/dt(t=0) = 0$, the collapse time predicted by Eq. (11) is $t_{\rm clps} = W_0^2\left(N/\tilde{N}_{\rm max} - 1\right)^{-1/2}$], and noncollapsing at $N < \tilde{N}_{\rm max}$.

The actual maximum value of N, found numerically from Eq. (6) with $V_0 = 0$ (it gives the norm of the *Townes soliton* [40]), is

$$N_{\max} = 5.85 \approx 0.93\tilde{N}_{\max}, \tag{12}$$

which characterizes the accuracy of the VA. For the condensate of ^{7}Li atoms, a typical collapse threshold corresponds to the number of atoms $\lesssim 10^4$.

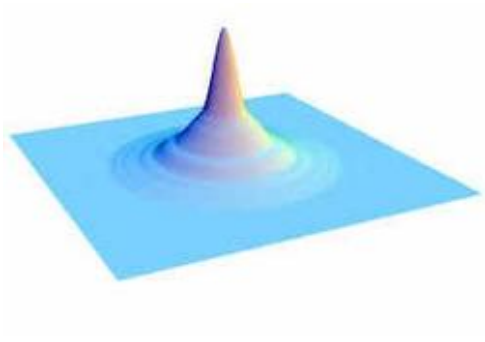

Equation (11) helps one to understand what may happen to the 2D soliton under the action of the weak "management", with $\varepsilon/2 \ll 1$. First, for $\varepsilon = 0$, Eq. (11) predicts a stable equilibrium position, which is given by a smaller root of equation

$$W_0^4 \exp\left(-W_0^2\right) = \frac{1 - N/\tilde{N}_{\max}}{4V_0} \tag{13}$$

(the larger root gives an unstable solution). Then, the linearization of Eq. (11) (still with $\varepsilon = 0$) yields the eigenfrequency of small oscillations around $W = W_0$,

$$\omega_0 = \frac{\sqrt{2\left(1 - N/\tilde{N}_{\max}\right)\left(2 - W_0^2\right)}}{W_0^2}. \tag{14}$$

For instance, in the example considered below (Fig. 8), with $1 - N/\tilde{N}_{\max} = 0.155$ and $V_0 = 0.25$, the relevant root of Eq. (13) is $W_0 \approx 0.71$, and Eq. (14) yields $\omega_0 \approx 1.35$. Keeping quadratic and cubic terms in the expansion of Eq. (11) in powers of $w(t) \equiv W(t)/W_0 - 1$ around W leads to a standard equation of driven nonlinear oscillations.

In particular, in the near-critical situation, i.e., for $1 - N/\tilde{N}_{\max} \ll 1$, this equation takes the form of

$$\frac{d^2 w}{dt^2} + 16 V_0 w - 24 V_0 w^2 + 40 V_0 w^3 = -2\varepsilon V_0 \cos(\omega t) - 2\varepsilon V_0 \cos(\omega t)\, w. \tag{15}$$

It predicts the lowest-order direct resonance when ω is close to ω_0,the parametric resonance at ω close to $2\omega_0$, and higher-order resonances at $\omega = n\omega_0$, with $n = 2, 3, 4, ..$ [41]. The resonances may help to *stabilize* the 2D soliton against the collapse, as, increasing the amplitude of its intrinsic oscillations, the soliton spends less time in the "dangerous zone" with small width, that might be a starting point for the collapse. On the other hand, effectively stretching the soliton, the resonances may *destabilize* it against decay into radiation, at smaller values of N.

Both trends are observed in numerical simulations, as shown below. Comparison of predictions following from a numerical solution of full variational equation (11) and direct simulations of Eq. (6) is presented in the next section.

Method

Systematic simulations of Eq. (6) were performed by means of the split-step method [43], in the (x, y) domain of size 256×256 or 512×512. The simulations were run with the Gaussian initial configuration,

$$\Psi(x, y, 0) = A_0 \exp\left(-q\left[(x - x_0)^2 + (y - y_0)^2\right]\right), \; q > 0, \quad (16)$$

whose norm is $N = \pi A_0^2/q$ [cf. ansatz (8)]. Taking $N < N_{\max}$, as well as N slightly *exceeding* $N_{\max}$ [recall $N_{\max}$, the critical value of the norm for the onset of the free-space collapse, is given by Eq. (12)], it was quite easy to find stable solitons which keep their shape despite the temporal modulations imposed by the "management", see generic examples in Figs. 3 and 4. The former figure presents comparison of the initial and final shapes of the soliton, while the latter one displays the evolution of the soliton's amplitude in the course of its self-adjustment to the stable shape.

Comparison of the initial and final shapes of the soliton:

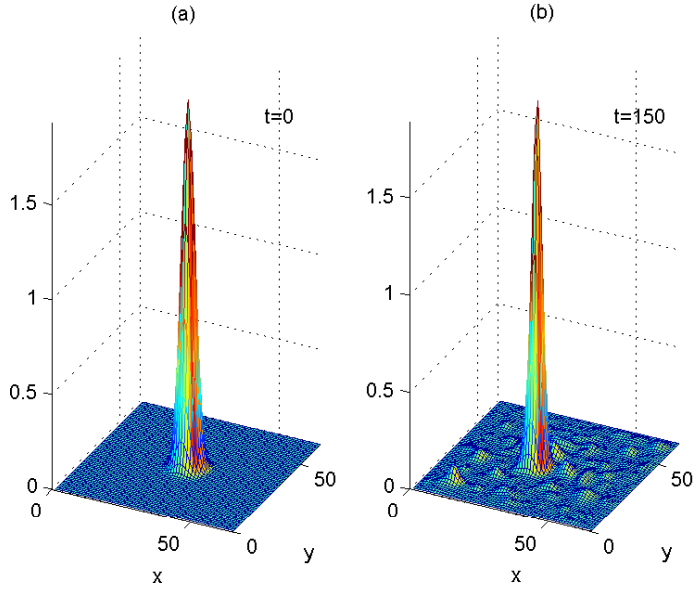

Figure: 3. A typical example of a stable 2D soliton, as obtained from the numerical solution of Eq.(6) with $V_0 = 0.65$, $\varepsilon = 0.5$, $\omega = 1.35$, and initial configuration (16) with $A_0 = 1.39$, $q = 0.5$, whose norm, $N = 6.07$, *exceeds* the collapse threshold in the static model, $N_{\max} \approx 5.85$. The panels display the density distribution, $|\Psi(x, y, t)|^2$, at $t = 0$ (a) and $t = 150$ (b).

Evolution of the soliton's amplitude:

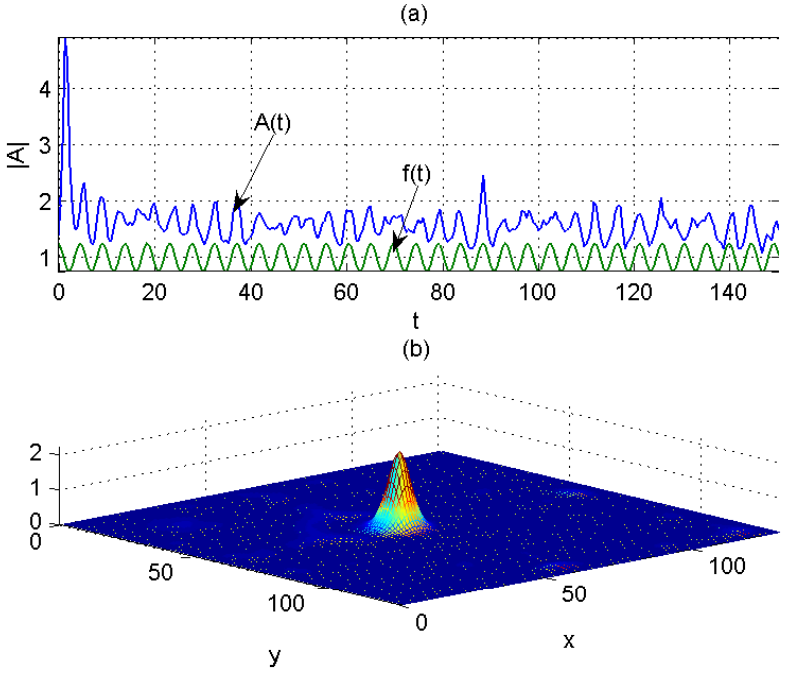

Figure: 4. (a) The evolution of the amplitude of the stable soliton, $|A| \equiv |\Psi(x = x_0, y = y_0)|$, for the same parameters as in Fig. 3, except for $V_0 = 0.5$ ($|A|$ has the same meaning in other figures). Curve $f(t)$ shows the modulation function in Eq.(6), $1 + (\varepsilon/2)\sin(\omega t)$; (b) The shape of the soliton at $t = 150$.

The soliton shapes displayed in Figs. 3 and 4 are confined, essentially, to a single cell of the OL (similar to results reported in previous works [4, 6, 8]). Roughly the same shapes would be observed in a parabolic trapping potential; however, the difference is that, if the nonlinearity is too weak, the OL cellular potential cannot suppress the tunnel decay of the localized pulses [37], therefore the decay is observed at smaller values of N, as shown below.

As said above, in the 2D equation with $V_0 = 0$ localized configurations with $N > N_{\max} = 5.85$ suffer collapse, while those with $N < N_{\max}$ decay. The static OL stabilizes 2D solitons in the latter case, but it cannot arrest the collapse of initial localized states with $N > N_{\max}$ [4, 5, 6]. The numerical analysis of the model with the quasi-1D lattice potential subjected to the periodic time modulation did not reveal stable solitons with $N > N_{\max}$ either [33]. As shown in the following Fig. 5, in the present model the periodic time modulation of the two-dimensional OL potential makes it possible to stabilize the solitons both at $N < N_{\max}$ and in some interval *above* $N_{\max}$. The actual increase of critical norm is not large, but the very fact that the constraint $N \leq N_{\max}$ can be broken is an interesting result, as it has never been reported before, to the best of our knowledge.

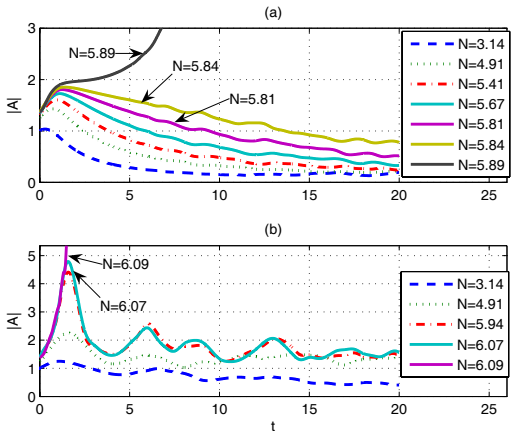

Figure: 5. The evolution of the soliton's amplitude, as obtained from the numerical solution of Eq. (6) for $\varepsilon = 0.5$ and $\omega = 1$ and different values of norm N of initial configuration (16) (higher curves correspond to larger N). (a) The model without the optical lattice, $V_0 = 0$. In this case, all configurations with $N < N_{\max} \approx 5.85$ decay, while the ones with $N > N_{\max}$ suffer the collapse. (b) In the presence of the time-modulated optical lattice with $V_0 = 0.5$, the 2D solitons may be stable, including some values of N *above* $N_{\max}$. In particular, the soliton is stable at $N = 6.01 \approx 1.03 N_{\max}$, while it collapses for $N = 6.09$, at $t = 1.49$. If N is too small, $N < N_{\min}$, the soliton gradually decays into radiation. In panel (b), the curve for $N = 3.14$, which is slightly smaller than the corresponding value of $N_{\min}$, also shows the slow decay of the soliton.

Comparison of the predictions of the VA with numerical results in two typical cases (for stable and decaying solitons, corresponding to $N = 5.4$ and $N = 4.6$, respectively). The discrepancy in the dependence of the soliton's amplitude on time, observed in the former case, is a known feature [42, 39, 18], explained by the fact that the oscillations predicted by the VA *are damped by the radiation loss*, which *is not taken into regard by the VA* Eq.(8).

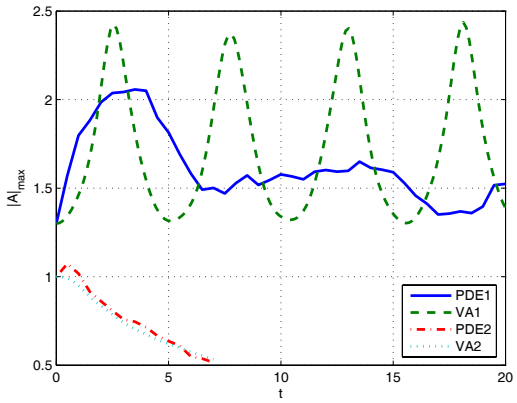

Figure: 7. Comparison of the evolution of the soliton's amplitude, as predicted by the variational approximation ("VA") and found from direct simulations of the partial differential equation (6) ("PDE"), for $N = 5.4$ (a stable soliton) and $N = 4.6$ (a decaying state).

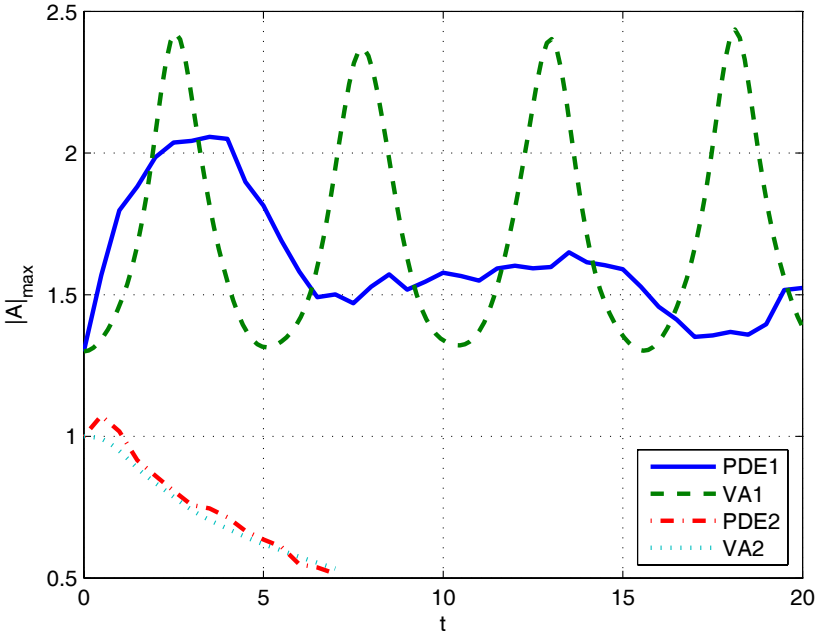

Figure: 7. Comparison of the evolution of the soliton's amplitude, as predicted by the variational approximation ("VA") and found from direct simulations of the partial differential equation (6) ("PDE"), for $N = 5.4$ (a stable soliton) and $N = 4.6$ (a decaying state).

The VA predicts eigenfrequency ω_0 of intrinsic oscillations of the weakly perturbed 2D soliton trapped in the static OL, see Eq. (14). Because this feature may be important to understand the response of the soliton to the periodic time modulation of the lattice, in terms of possible resonances (see below), it is necessary to check whether the presence of the eigenfrequency is confirmed by simulations of full equation (6) with the static lattice, i.e., $\varepsilon = 0$.

Random perturbations

In the Fig. 8 we display the power spectrum of small oscillations around the soliton caused by the addition of a small random perturbation to it, for $V_0 = 0.25$ and $N = 5.31$, which corresponds to $1 - N/\tilde{N}_{\max} \approx 0.155$. As mentioned above, in this case Eqs. (13) and (14) predict the eigenfrequency to be $\omega_0 \approx 1.35$.

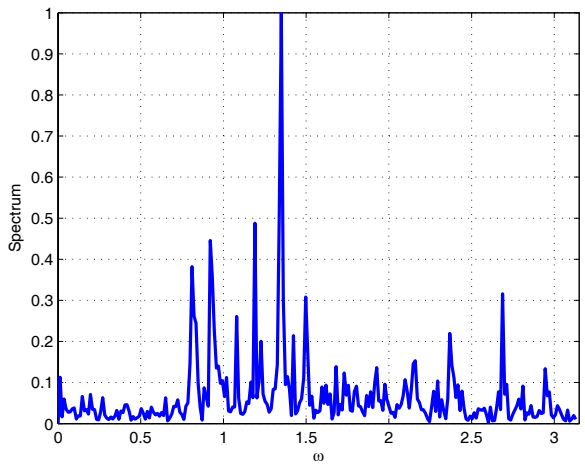

Figure: 8. The power spectrum of small random perturbations around the stable soliton trapped in the static lattice ($\varepsilon = 0$), for $V_0 = 0.25$ and $N = 5.31$.

Random perturbations

The spectrum in Fig. 8 clearly shows the main peak quite close to this point. Peaks corresponding to higher-order resonances (see above) can also be recognized in the figure. To produce the spectrum shown in Fig.8, we simulated the evolution of the soliton up to a very long time, $t = 1200$, eliminating a contribution from a relatively short initial stage, which featured a transient behavior.

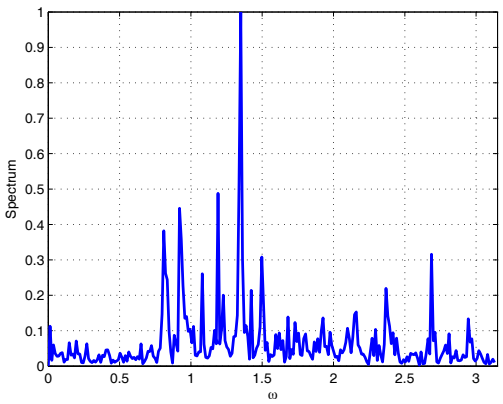

Figure: 8. The power spectrum of small random perturbations around the stable soliton trapped in the static lattice ($\varepsilon = 0$), for $V_0 = 0.25$ and $N = 5.31$.

Stability

Results produced by the systematic numerical analysis of the stability of the 2D soliton under the action of the "lattice management" are collected in the following Fig. 10(a), which displays the stability region in the plane of the modulation parameters, ω and ε, for fixed $V_0 = 0.25$ and $N = 5.905$. Note that this norm again (like in the cases of Figs. 3 and 4) slightly exceeds the collapse threshold in the static model, which is given by Eq. (12). The stability region in the plane of ε and N, for the same OL strength, $V_0 = 0.25$, as in Fig. 10, and $\omega = 4$, is displayed in Fig. 10(b). The latter plot explicitly demonstrates the *growth* of the collapse threshold, $N_{\max}$, with the increase of the modulation amplitude. Note that not the entire parameter region below the stability border in Fig. 10(b) corresponds to stable solitons; if N is too small, the solitons are unstable against decay, see below.

Stability diagrams

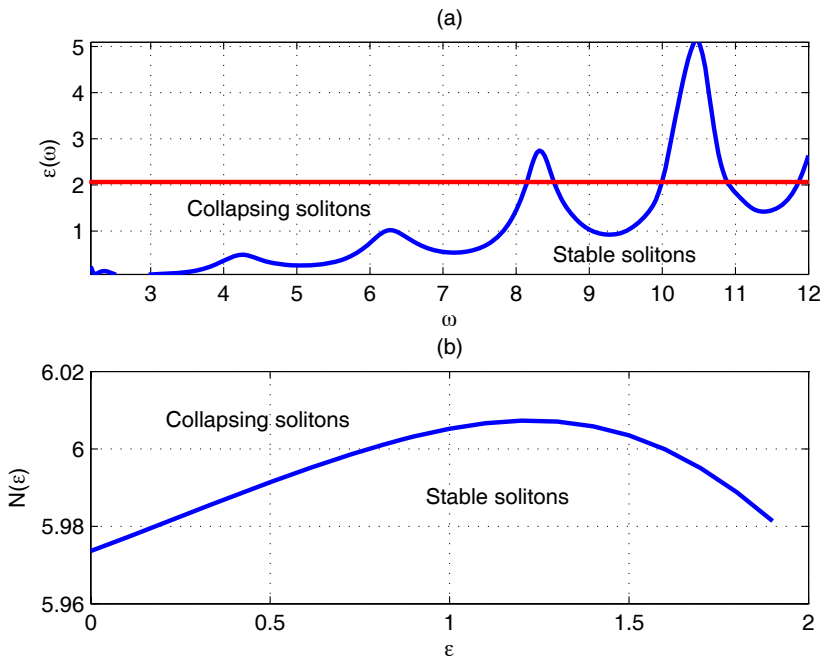

Figure: 10. (a) The stability region in the plane of the modulation parameters, ω and ε, for $V_0 = 0.25$ and $N = 5.905$. The area relevant to the model with the periodically modulated optical lattice corresponds to $\varepsilon \leq 2$, where the time-dependent amplitude in Eq. (6), $1 + (\varepsilon/2)\cos(\omega t)$, does not change its sign. (b) The collapse threshold versus the modulation amplitude, ε, for $V_0 = 0.25$ and $\omega = 4$.

In Fig. 10(a), the horizontal line denotes the maximum possible value of the modulation amplitude in the model of the time-modulated OL, $\varepsilon_{\text{max}} = 2$. A noteworthy fact is that the stability region can extend up to this limit, i.e., 100% modulation depth (recall that, in the case when the stabilization of 2D solitons was provided by the quasi-1D lattice, the stability limit corresponded to shallow modulation [33]). The results for $\varepsilon > 2$ are included too in Fig. 10(a), as they may find a different physical realization, corresponding to a superposition of moving OLs [34].

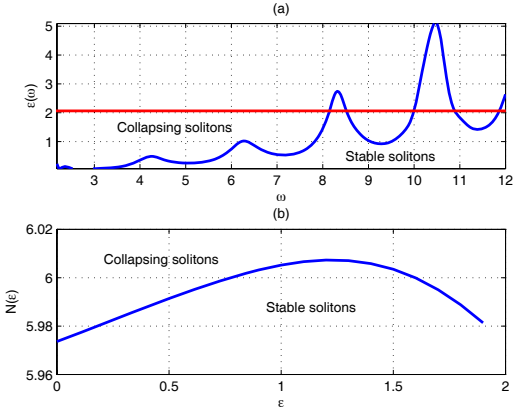

Figure: 10.

A feature obvious in Fig. 10(a) is a resonant-like dependence of the stability border on ω. This may be a manifestation of the fundamental resonance at ω close to ω_0 and higher-order resonances at multiple values of ω. As argued above, the resonance may help to arrest the collapse, by forcing the vibrating soliton to spend less time in the state where it is "dangerously" narrow.

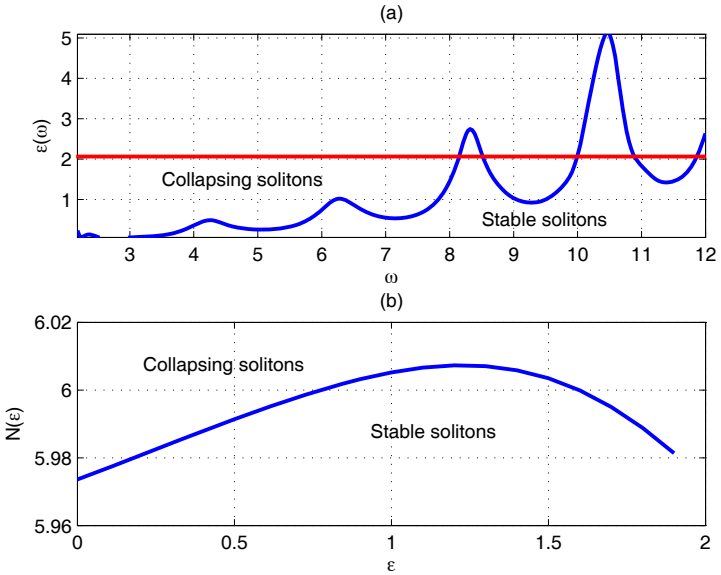

Figure: 10.

Since the value of the norm corresponding to Fig. 10(a) is close to $N_{\max}$, one may expect that the corresponding fundamental-resonance frequency should be close to one given by Eq. (15), i.e., $\omega_0 = 2$, for $V_0 = 0.25$ [the same is given by Eqs. (13) and (14) in the limit of $N/\tilde{N}_{\max} \to 0$]. Indeed, the picture in Fig. 10(a) is consistent with the expectation of the fundamental and higher-order resonances at $\omega = n\omega_0$, $n = 1, 2, 3, 4$ (the picture also suggests the existence of a very strong resonance close to $\omega = 5\omega_0$, but that one falls deeply into the unphysical region, $\varepsilon > 2$).

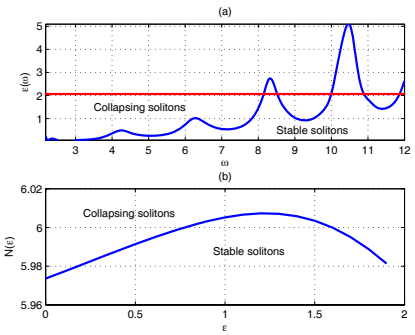

Figure: 10.

As mentioned above, the soliton whose norm is too small cannot stabilize itself and decays into quasi-linear waves. Therefore, along with the upper stability boundary, $N = N_{\max}$, that guarantees the absence of the collapse, it is necessary to identify the lower one, $N = N_{\min}$, which secures the stability of the soliton against the decay. Both boundaries, as predicted by the VA and found from the direct simulations, are displayed in Fig. 15, in the form of dependences $N_{\max}(V_0)$ and $N_{\min}(V_0)$, at fixed $\varepsilon = 0.5$ for several different values of ω. In each panel, the stability region is $N_{\min} < N < N_{\max}$.

Stability boundaries

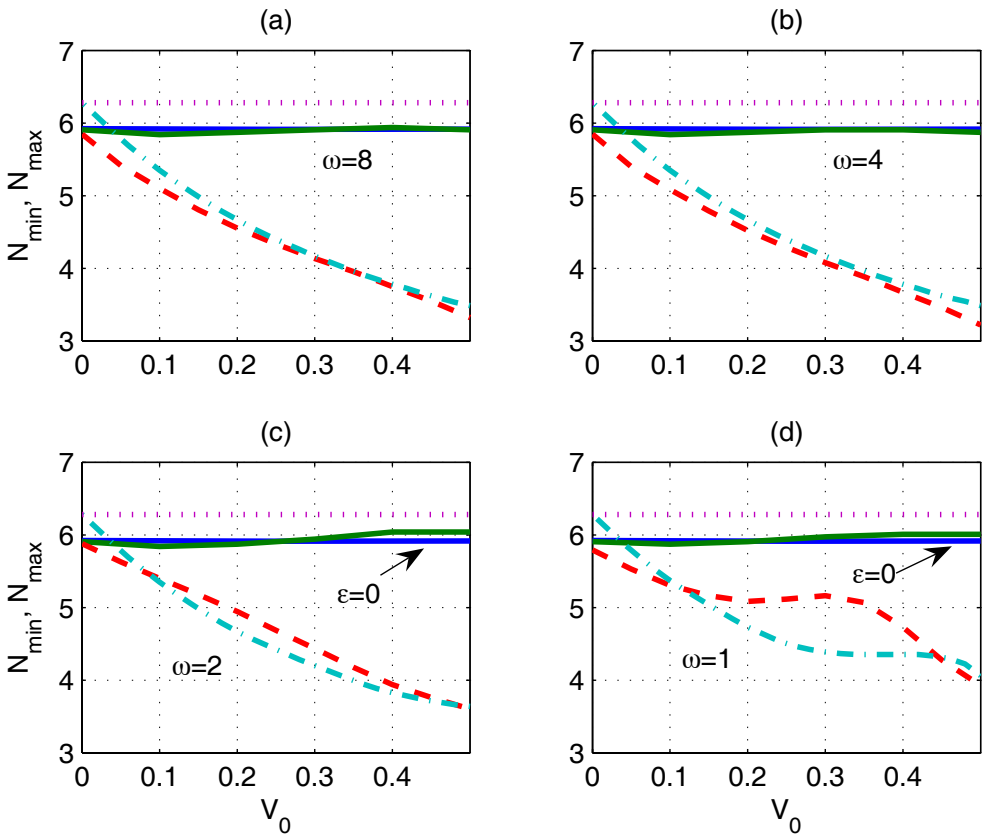

Figure: 15. The dependence of the stability boundaries, $N_{\max}$ and $N_{\min}$, on the OL strength, V_0, at $\varepsilon = 0.5$ and different values of the modulation frequency, ω.

Stability boundaries

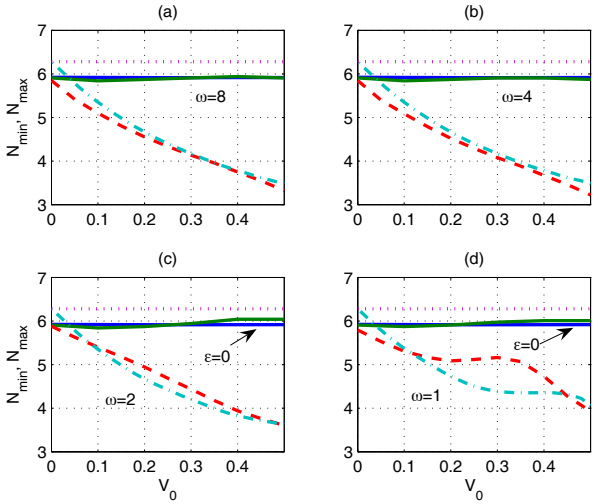

Figure: 15. The dependence of the stability boundaries, $N_{\max}$ and $N_{\min}$, on the OL strength, V_0, at $\varepsilon = 0.5$ and different values of the modulation frequency, ω. Solid and dashed lines show, severally, $N_{\max}$ and $N_{\min}$ as found from the simulations, while the dotted and dashed-dotted lines represent, respectively, $N_{\max}$ and $N_{\min}$ as predicted by the *variational approximation (VA)*. The arrows in (c) and (d) indicate values $N_{\max}$ for the stationary case, $\varepsilon = 0$.

We observe in Fig. 15 that dependences $N_{\min}(V_0)$ produced by the VA are in reasonable agreement with the results of direct simulations of the GPE for modulation frequencies $\omega \geq 2$. However, there is a conspicuous discrepancy between the VA and GPE for ω close to 1. On the other hand, this range features strong resonances in the perturbation spectrum, see Fig. 8. Therefore, it is interesting to explore the $N_{\min}(V_0)$ dependence in region $0.5 < \omega < 2$, where the resonances may lead to decay of the soliton.

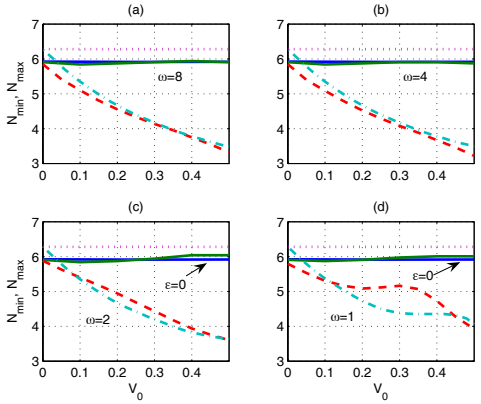

Figure: 15.

These results are displayed in the Fig. 18, which shows that plots $N_{\min}(V_0)$ essentially differ, in this region, from their counterparts both in the static model (see the curve for $\varepsilon = 0$ in Fig. 18) and in the high-frequency region, $\omega \geq 2$: actually, $N_{\min}$ increases due to the resonant decay of the solitons. The fact that the resonances are narrow enough, as seen in Fig. 8, may explain a non-monotonous character of dependences $N_{\min}(V_0)$ for $\omega = 1.10$ and 1.25.

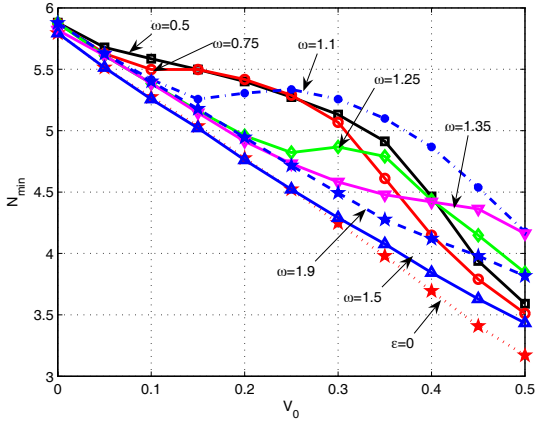

Figure: 18.

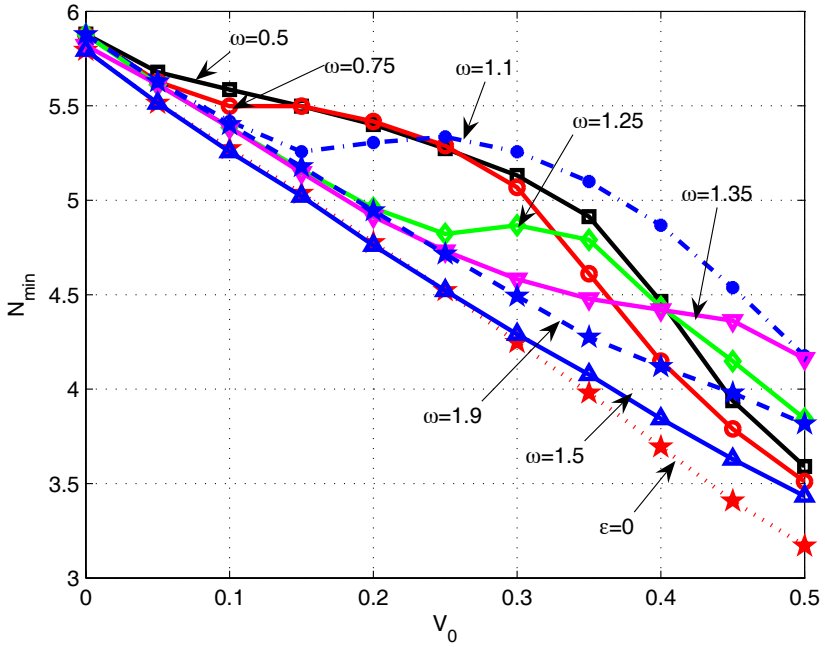

Figure: 18. Dependencies $N_{\min}(V_0)$ for $\varepsilon = 0.5$ and different modulation frequencies ω in the resonant area, $0.5 < \omega < 2$. The curve pertaining to $\varepsilon = 0$ (the static model) is included for comparison.

Dependencies of $N_{\max}$ and $N_{\min}$ on the modulation frequency are displayed in Fig. 20, for the same modulation amplitude as above, $\varepsilon = 0.5$, and several different values of V_0. It is quite natural that dependencies $N_{\min}(\omega)$, as predicted by the VA and generated by direct simulations of Eq. (6), are close to each other for smaller values of the OL strength, $V_0 = 0.1$ and 0.25, while at $V_0 = 0.5$ the discrepancy between them is considerable. Non-monotonous behavior of $N_{\min}(\omega)$ in resonant zone $0.5 < \omega < 2$, which correlates to peculiarities of dependencies $N_{\min}(V_0)$ in the same zone.

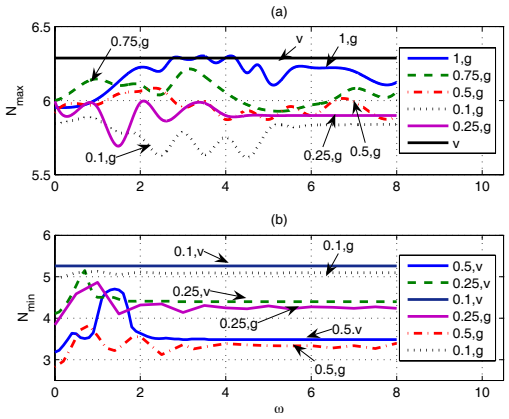

Figure: 20. The dependence of the stability boundaries

Stability boundaries

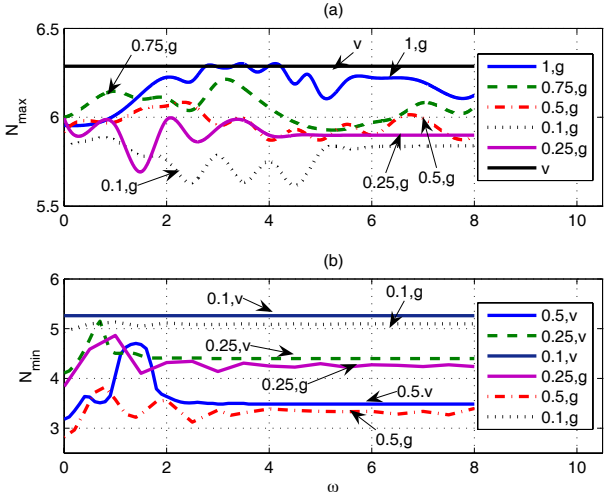

Figure: 20. The dependence of the upper (a) and lower (b) stability boundaries, $N_{\max}$ and $N_{\min}$, on modulation frequency ω for $\varepsilon = 0.5$ and different values of OL strength V_0, which are specified in the box. Labels "v" and "g" pertain, severally, to the curves predicted by the variational approximation and those found from direct simulations of Gross-Pitaevskii equation (6) (the VA predicts flat value $\tilde{N}_{\max} = 2\pi$, see text). The arrows identify those curves which may seem indisnguishable in the black-and-white rendition of the figure.

Optical periodic and quasiperiodic lattice.

$$i\frac{\partial \Phi}{\partial \tau} = [-\nabla_2^2 + V(\mathbf{r}) + G\,|\Phi|^2]\Phi, \tag{17}$$

We consider a quasiperiodic *Penrose tiling* trapping potential V of the following form,

$$V = V(x, y, \tau) = V_c + \varepsilon \sum_{n=1}^{N} \cos(\mathbf{k}^{(n)}\mathbf{r} + \pi\theta(\tau)) = \tag{18}$$

$$V_c + \varepsilon(1 - 2\theta(\tau)) \sum_{n=1}^{N} \cos(\mathbf{k}^{(n)}\mathbf{r}), \tag{19}$$

where $\mathbf{k}^{(n)} = \{\cos(2\pi(n-1)/N, \sin(2\pi(n-1)/N\}$, $V_c = const$, and the *time-dependence* appears through the pulse function $\theta(\tau) = \mathbf{1}$ for $(2n+1)\,T_t < \tau \leq (2n+2)\,T_t$ and $\theta(\tau) = \mathbf{0}$ otherwise, T_t is a time period, $n = 0, 1, 2....$

Optical periodic and quasiperiodic lattice. Repulsive interaction.

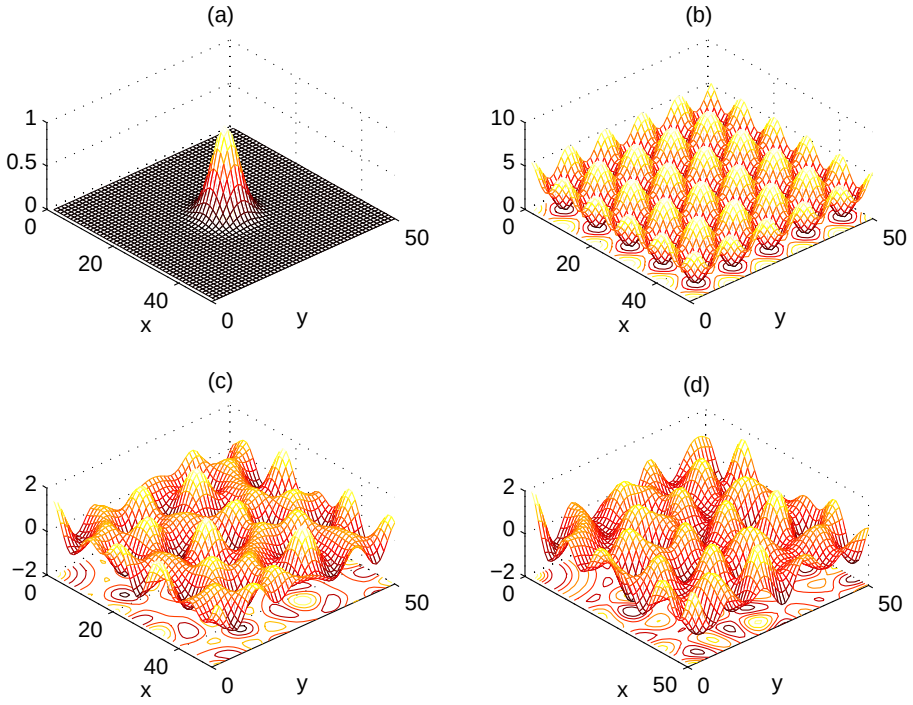

Figure: (a) Init Gaussian package. (b),(c),(d) two-dimensional distribution of the trapping potential $V(x, y, 0)$ induced by optical lattices (OL) for Penrose tiling (a pattern of tiles, which completely cover an infinite plane in an aperiodic manner) for cases (b) $N = 4$; (c) $N = 5$; (d) $N = 7$.

Repulsive interaction case, N=4

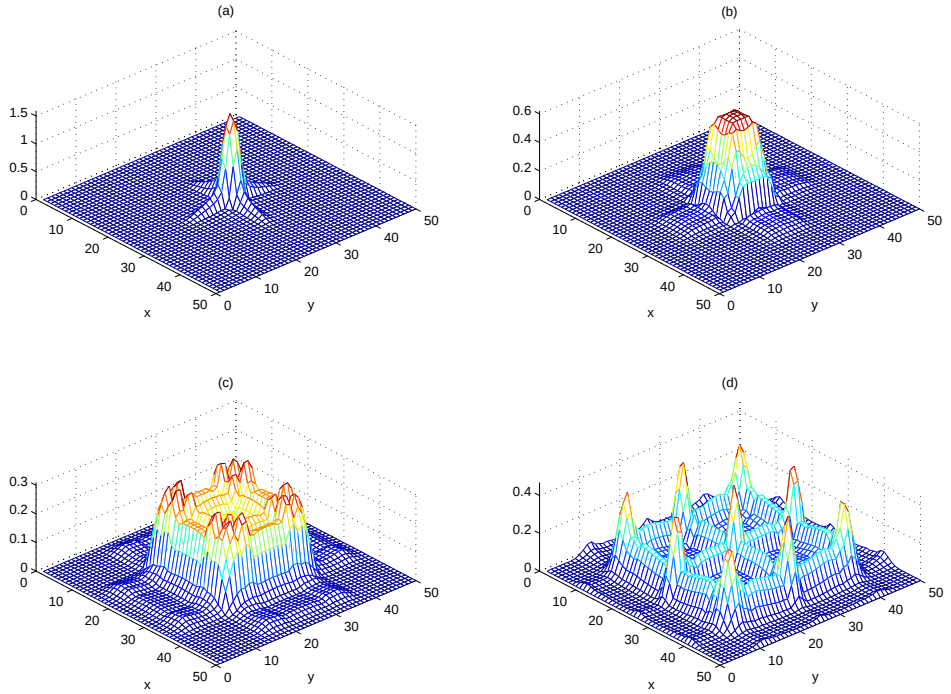

Figure: 22. Evolution of BEC soliton for period π-phase shift $T_t = 50$ and different times: (a) $\tau = 40$; (b) $\tau = 80$; (c) $\tau = 120$; (d) $\tau = 160$.

Repulsive interaction case, N=5

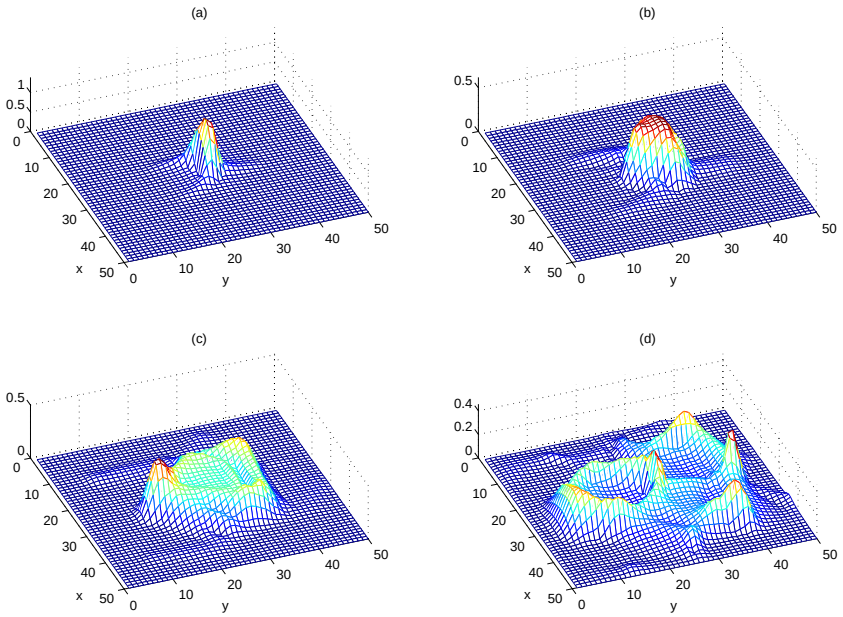

Figure: 23. The same as in Fig.22, except $N = 5$ in trapping potential $V(x, y, \tau)$. [*G. Burlak, A. Klimov. The solitons redistribution in Bose-Einstein condensate in quasiperiodic optical lattice. Physics Letters A. 369/5-6, 510-517 (2007).*]

Repulsive interaction case, N=7

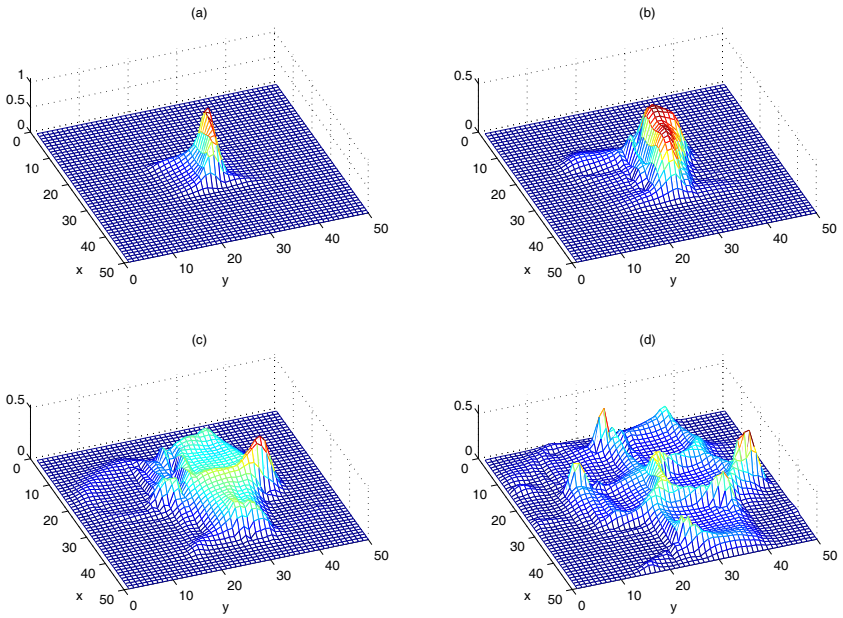

Figure: The same as in Fig.22, except $N = 7$ in trapping potential $V(x, y, \tau)$.

Conclusion 1.

We have studied the dynamics of 2D solitons in the model of BEC trapped in the square-shaped OL (optical lattice) whose strength it subject to the periodic time modulation. Being quite feasible for the experimental implementation, the model belongs to a broad class of schemes of the periodic management of solitons [24].

By means of the VA (variational approximation) and direct systematic simulations of the underlying Gross-Pitaevskii equation, we have identified stability regions for the solitons in the parameter space of the model, including both maximum and minimum values of the norm, as summarized in Figs. 10, 15, 18 and 20.

Conclusion 2.

A remarkable feature demonstrated by these results is that *the stability limit may reach the maximum (*100%*) modulation depth*. It is noteworthy too that an *increase* of the collapse threshold in predicted in comparison with its classical value in the static situation, which corresponds to the norm of the Townes soliton.

The stability borders predicted by the VA are found to be in reasonable agreement with the numerical results. In the plane of the modulation frequency and amplitude, the stability boundary features a salient resonant structure, which may also be qualitatively explained by means of the VA.

Conclusion 3.

The analysis reported in this Report can be extended in several directions. It may be interesting to study interactions between the solitons in this setting, and identify stability limits for vortex solitons, as well as for 2D gap solitons in the model combining the repulsive nonlinearity and lattice management.

Another extension may be made in the direction of an anisotropic lattice management, i.e., applying time modulations shifted by π to the two 1D sublattices.

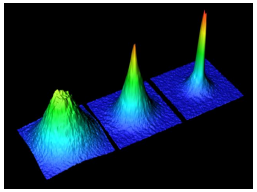

Some references:

- F. Calogero, A. Degasperis, Spectral transform and solitons, Elsevier Science Ltd (1982); S.Novikov,S.V.Manakov,L.P.Pitaevskii, V.E. Zakharov, Theory of Solitons: The Inverse Scattering Method, (1984).
- B. A. Malomed, D. Mihalache, F. Wise, and L. Torner, J. Optics B: Quant. Semics. Opt. **7**, R53 (2005).
- K. E. Strecker, G. B. Partridge, A. G. Truscott, and F. G. Hulet, Nature **417**, 150 (2002); L. Khaykovich, F. Schreck, G. Ferrari, T. Bourdel, J. Cubizolles, L. D. Carr, Y. Castin, and C. Salomon, Science **296**, 1290 (2002); S. L. Cornish, S. T. Thompson, and C. E. Wieman, Phys. Rev. Lett. **96**, 170401 (2006).
- B. B. Baizakov, B. A. Malomed, and M. Salerno, Europhys. Lett. **63**, 642 (2003); J. Yang and Z. H. Musslimani, Opt. Lett. **28**, 2094 (2003).

- B. B. Baizakov, B. A. Malomed and M. Salerno, Phys. Rev. A **70**, 053613 (2004).
- B. B. Baizakov, B. A. Malomed and M. Salerno, in: *Nonlinear Waves: Classical and Quantum Aspects*, ed. by F. Kh. Abdullaev and V. V. Konotop, pp. 61-80 (Kluwer Academic Publishers: Dordrecht, 2004); also available at http://rsphysse.anu.edu.au/~asd124/Baizakov_2004_61_NonlinearWa
- J. Kasprzak, M. Richard, S. Kundermann, A. Baas, P. Jeambrun, J. M. J. Keeling, F. M. Marchetti, M. H. Szymanska, R. Andre, J. L. Staehli, V. Savona, P. B. Littlewood, B. Deveaud, and L. S. Dang, Nature **443**, 409 (2006).
- D. Mihalache, D. Mazilu, F. Lederer, Y. V. Kartashov, L.-C. Crasovan, and L. Torner, Phys. Rev. E **70**, 055603(R) (2004).

- O. Zobay, S. Pötting, P. Meystre, and E. M. Wright, Phys. Rev. A **59**, 643 (1999); F. Kh. Abdullaev, B. B. Baizakov, S. A. Darmanyan, V. V. Konotop, and M. Salerno, *ibid*. **64**, 043606 (2001); A. Trombettoni, and A. Smerzi, Phys. Rev. Lett. **86**, 2353 (2001); G. L. Alfimov, V. V. Konotop, and M. Salerno, Europhys. Lett. **58**, 7 (2002).
- K. M. Hilligsøe, M. K. Oberthaler, and K.-P. Marzlin, Phys. Rev. A **66**, 063605 (2002); D. E. Pelinovsky, A. A. Sukhorukov, and Y. S. Kivshar, Phys. Rev. E **70**, 036618 (2004).
- B. Eiermann, Th. Anker, M. Albiez, M. Taglieber, P. Treutlein, K.-P. Marzlin, and M. K. Oberthaler, Phys. Rev. Lett. **92**, 230401 (2004).
- O. Morsch, M. Oberthaler, Rev. Mod. Phys. 78, 179215 (2006).

- B. B. Baizakov, V. V. Konotop, and M. Salerno, J. Phys. B: At. Mol. Opt. Phys. **35**, 5105 (2002); P. J. Y. Louis, E. A. Ostrovskaya, C. M. Savage, and Y. S. Kivshar, Phys. Rev. A **67**, 013602 (2003); E. A. Ostrovskaya and Y. S. Kivshar, Opt. Exp. **12**, 19 (2004); Phys. Rev. Lett. **93**, 160405 (2004); H. Sakaguchi and B. A. Malomed, J. Phys. B **37**, 2225 (2004); A. Gubeskys, B. A. Malomed, I. M. Merhasin, Phys. Rev. A **73**, 023607 (2006).
- B. B. Baizakov, B. A. Malomed, and M. Salerno, Eur. Phys. J. D **38**, 367 (2006).
- H. Sakaguchi, B. A. Malomed, Phys. Rev. E 74, 026601 (2006).
- P. Pedri and L. Santos, Phys. Rev. Lett. **95**, 200404 (2005).
- I. Tikhonenkov, B. A. Malomed, and A. Vardi, Phys. Rev. Lett. **100**, 090406 (2008).

- H. Saito and M. Ueda, Phys. Rev. Lett. **90**, 040403 (2003); F. Kh. Abdullaev, J. G. Caputo, R. A. Kraenkel, and B. A. Malomed, Phys. Rev. A **67**, 013605 (2003); G. D. Montesinos, V. M. Pérez-García, and H. Michinel, Phys. Rev. Lett. **92**, 133901 (2004).
- I. Towers and B. A. Malomed, J. Opt. Soc. Am. **19**, 537 (2002).
- K. Staliunas, S. Longhi, and G. J. de Valcárcel, Phys. Rev. A 70, 011601(R) (2004).
- M. Trippenbach, M. Matuszewski, and B. A. Malomed, Europhys. Lett. **70**, 8 (2005); M. Matuszewski, E. Infeld, B. A. Malomed, and M. Trippenbach, Phys. Rev. Lett. **95**, 050403 (2005).

- V. A. Brazhnyi and V. V. Konotop, Phys. Rev. A **72**, 033615 (2005); M. A. Porter, M. Chugunova and D. E. Pelinovsky, Phys. Rev. E 74, 036610 (2006).
- P. G. Kevrekidis, G. Theocharis, D. J. Frantzeskakis, and B.A. Malomed, Phys. Rev. Lett. **90**, 230401 (2003).D. E. Pelinovsky, P. G. Kevrekidis, and D. J. Frantzeskakis, *ibid*. **91**, 240201 (2003); F. Kh. Abdullaev, R. M. Galimzyanov, M. Brtka, and R. A Kraenkel, J. Phys. B: At. Mol. Opt. Phys. **37** (2004) 3535 (2004).
- B. A. Malomed. *Soliton Management in Periodic Systems* (Springer: New York, 2006).
- A. Itin, T. Morishita, and S. Watanabe, Phys. Rev. A 74, 033613 (2006).

- C. Tozzo, M. Krämer, and F. Dalfovo, Phys. Rev. A 72, 023613 (2005); M. Krämer, C. Tozzo, and F. Dalfovo, Phys. Rev. A **71**, 061602(R) (2005).
- T. Mayteevarunyoo and B. A. Malomed, Phys. Rev. A **74**, 033616 (2006).
- C. Schori, T. Stöferle, H. Moritz, M. Köhl, and T. Esslinger, Phys. Rev. Lett. **93**, 240402 (2004).
- J. J. G. Ripoll and V. M. Pérez-García, Phys. Rev. A 59, 2220 (1999); J. J. García-Ripoll, V. M. Pérez-García, and Pedro Torres, Phys. Rev. Lett. **83**, 1715 (1999); B. Baizakov, G. Filatrella, B. Malomed, and M. Salerno, Phys. Rev. E **71**, 036619 (2005); P. Engels, C. Atherton, and M. A. Hoefer, Phys. Rev. Lett. **98**, 095301 (2007); Yu. Kagan and L. A. Manakova, Phys. Rev. A **76**, 023601 (2007).

- K. Staliunas, S. Longhi, and G. J. de Valcárcel, Phys. Rev. Lett. **89**, 210406 (2002); Phys. Rev. A **70**, 011601(R) (2004).
- P. Engels, C. Atherton, and M. A. Hoefer, Phys. Rev. Lett. **98**, 095301 (2007).
- H. Saito, R. G. Hulet, and M. Ueda, Phys. Rev. A 76, 053619 (2007); H. Susanto, G. K. Kevrekidis, B. A. Malomed, and F. Kh. Abdullaev, Phys. Lett. **372**, 1631 (2008).
- T. Mayteevarunyoo, B. A. Malomed, and M. Krairiksh, Phys. Rev. A **76**, 053612 (2007).
- K. Staliunas, R. Herrero, and G. J. de Valcárcel, Phys. Rev. A **75**, 011604(R) (2007).
- K. Staliunas, R. Herrero, and G. J. de Valcárcel, Phys. Rev. E **73**, 065603(R) (2006).
- G. Burlak and A. Klimov, Phys. Lett. A **369**, 510 (2007).

- B. B. Baizakov and M. Salerno, Phys. Rev. A **69**, 013602 (2004).
- M. Desaix, D. Anderson, M. Lisak, J. Opt. Soc. Am. B **8**, 2082 (1991).
- V. M. Pérez-García, H. Michinel, J. I. Cirac, M. Lewenstein, and P. Zoller, Phys. Rev. A **56**, 1424 (1997); B. A. Malomed, in Progress in Optics, vol. 43, p. 71, ed. by E. Wolf (Amsterdam: North-Holland, 2002).
- L. Bergé, Phys. Rep. **303**, 259 (1998).
- L. D. Landau and E. M. Lifshitz, *Mechanics*, 3rd ed. (Pergamon Press: Oxford, England, 1976).
- F. Kh. Abdullaev and J. G. Caputo, Phys. Rev. E **58**, 6637 (1998).

W. H. Press, S. A. Teukovsky, W. T. Vetterling, and B. P.Flannery, *Numerical recipes in C++* (Cambridge University Press: Cambridge, 2002).

W. L. Kath and N. F. Smyth, Phys. Rev. E **51**, 1484 (1995).

Notification: the most recent BEC -2010 (super-photons)!!!

Authors: Jan Klaers, Julian Schmitt, Frank Vewinger, Martin Weitz, *Institut für Angewandte Physik, Bonn, Germany*
Title: **Bose-Einstein condensation of photons in an optical microcavity**;
Journal: Nature 468, 545-548 (25 November 2010);

Upon increasing the photon density, we observe the following BEC signatures: the photon energies have a Bose Einstein distribution with *a massively populated ground-state mode* on top of a broad thermal wing; the phase transition occurs at the expected photon density and exhibits the predicted dependence on cavity geometry; and the ground-state mode emerges even for a spatially displaced pump spot.

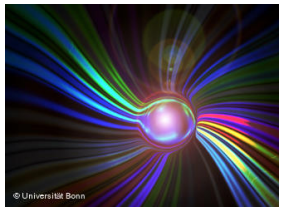

Thank you for attention!

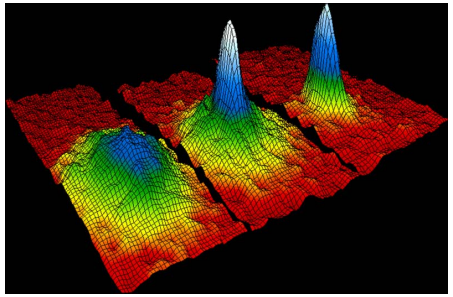

Figure: Velocity-distribution data of a gas of rubidium atoms, confirming the discovery of a new phase of matter, the BoseEinstein condensate